PULSE-STREAM MODELS IN ULTRASOUND IMAGING

Adrien Besson[⋆]*, Dimitris Perdios*[⋆]*, Marcel Arditi*[⋆]*, Yves Wiaux*[∗]*, Jean-Philippe Thiran*[⋆,†]

[⋆]Signal Processing Laboratory (LTS5), Ecole Polytechnique Fédérale de Lausanne, Switzerland
[∗]Institute of Sensors, Signals and Systems, Heriot-Watt University, UK
[†]Department of Radiology, University Hospital Center and University of Lausanne, Switzerland

ABSTRACT

This paper considers the problem of reconstructing ultrasound (US) element raw-data from random projections. It presents a new signal model, coined as *multi-channel ultrasound pulse-stream model*, which exploits the pulse-stream models of US signals and accounts for the inter-sensor dependencies. We propose a sampling theorem and a reconstruction algorithm, based on ℓ_1-minimization, for signals belonging to such a model. We show the benefits of the proposed approach through numerical simulations on 1D-signals and on in vivo carotid images.

Index Terms— Compressed sensing, sparsity, ultrasound imaging

1. INTRODUCTION

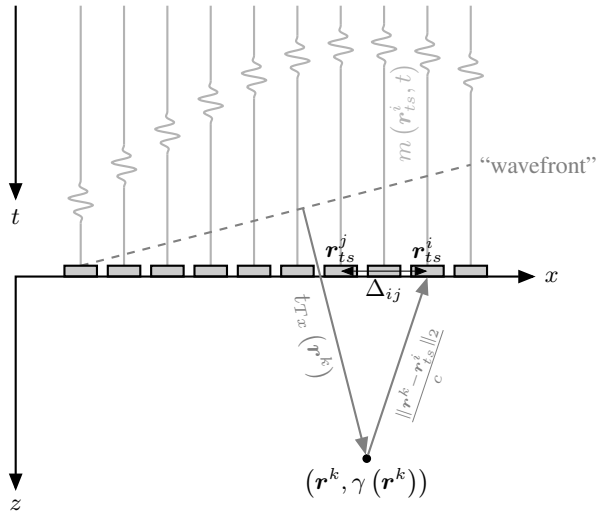

Fig. 1: Standard 2D ultrasound imaging configuration.

Pulse-echo ultrasound (US) imaging is based on the transmission of short acoustic pulses through the human body. When such pulses encounter medium inhomogeneities, part of their energy is reflected back to the array of transducer-elements. The received signals, denoted as element-raw data, consist of backscattered echoes from the medium. Ultrafast US imaging is one specific modality of pulse-echo imaging which exploits the transmission of plane waves (PW) or diverging waves in order to insonify the whole medium at once [1]. Formally, let us assume that the transducer array is made of N_{el} elements, positioned at $(\boldsymbol{r}_{ts}^p)_{p=1}^{N_{el}}$, as described on Figure 1. Let us also consider that the medium is made of K point-scatterers positioned at $\left(\boldsymbol{r}^k\right)_{k=1}^K$. The signal $m_p\left(t\right)$ received at the p-th element can be expressed as [2, 3]:

$$m_p\left(t\right) = \sum_{k=1}^{K} a_k h\left(t - t_p^k\right), \tag{1}$$

where a_k and t_p^k are the amplitude and delay of the k-th point-scatterer and $h\left(t\right)$ is the pulse. In the remainder of the paper, we will consider that the pulse is known and that it can be written as $h\left(t\right) = \left(e * h_{ea} * h_{ae}\right)\left(t\right)$, where $e\left(t\right)$ is the excitation signal, $h_{ea}\left(t\right)$ is the electro-acoustical impulse response of the transducer elementand $h_{ae}\left(t\right)$ is the acousto-electrical impulse response of the transducer element [4].

In the case of US imaging, it is possible to relate the time instant t_p^k to the positions of the point-scatterer $\boldsymbol{r}^k$ and the transducer element $\boldsymbol{r}_{ts}^p$ using the following relationship [5]:

$$t_p^k = t_{Tx}\left(\boldsymbol{r}^k\right) + t_{Rx}\left(\boldsymbol{r}^k, \boldsymbol{r}_{ts}^p\right), \tag{2}$$

where $t_{Tx}\left(\boldsymbol{r}^k\right)$ is the propagation delay in transmit [5, 6], and $t_{Rx}\left(\boldsymbol{r}^k, \boldsymbol{r}_{ts}^p\right) = \frac{\|\boldsymbol{r}^k - \boldsymbol{r}_{ts}^p\|_2}{c}$ is the propagation delay in receive, as described on Figure 1.

The notion of *pulse stream* has been introduced by Hedge and Baraniuk [7] and designates signals that can be expressed as a convolution between a K-sparse spike train and a F-sparse impulse response. Two main approaches for recovery of pulse-stream signals have been studied.

The first approach models the pulse stream using the finite rate of innovation (FRI) framework, which defines sampling theorems and kernels for impulse signals [8]. Indeed, pulse streams can be seen as parametric signals, entirely defined by the amplitudes and delays of the spike train and one may be able to recover the pulse streams with only $2K$ samples. Tur *et al.* [3] as well as Chernyakova *et al.* [2] have applied this framework to US imaging, leading to significant data-rate reduction.

The second approach, which is of interest in this work, exploits sparse representations in the context of the compressed-sensing (CS) framework [9]. Indeed, pulse streams are K-sparse in the dictionary made of circular shifts of the impulse response [10]. Thus, one may perfectly recover pulse streams from few samples using convex optimization algorithms or greedy approaches [7, 10, 11].

Formally, let us consider a pulse stream $\boldsymbol{z} \in \mathbb{R}^N$, such that $\boldsymbol{z} = \boldsymbol{h} * \boldsymbol{s}$ with $\boldsymbol{s} \in \mathbb{R}^N$ the K-sparse spike train and $\boldsymbol{h} \in \mathbb{R}^N$ the F-sparse impulse response.

This work was supported by the UltrasoundToGo RTD project (no. 20NA21_145911), funded by Nano-Tera.ch.

Definition 1 (Definition 2 of [7])**.** The pulse-stream model is defined as follows:

$$\mathcal{M}^{z}_{K,F} := \left\{ \boldsymbol{z} \in \mathbb{R}^N : \boldsymbol{z} = \boldsymbol{s} * \boldsymbol{h} \mid \boldsymbol{s} \in \mathcal{M}_K \text{ and } \boldsymbol{h} \in \mathcal{M}_F \right\}, \tag{3}$$

where $\mathcal{M}_K \subset \mathbb{R}^N$ and $\mathcal{M}_F \subset \mathbb{R}^N$ are restricted unions of L_K K-dimensional and L_F F-dimensional canonical subspaces, respectively.

For signals belonging to the pulse-stream model $\mathcal{M}^{z}_{K,F}$, Hedge and Baraniuk [7] have derived a sampling theorem where the number of measurements necessary for perfect reconstruction scales linearly with $K+F$ instead of KF (standard CS). In the proposed work, we apply the concept of pulse-stream models to US imaging described in the first part of this introduction. Starting from the model described in Equation (1), we consider inter-channel dependencies in order to derive an additional structure of the US signals. This structure, expressed as restrictions on the possible support of the US signals, leads us to define a new model, denoted as *multi-channel US pulse streams*, from which we present a sampling theorem and a recovery algorithm.

The remainder of the paper is organized as follows. In Section 2, the signal model is presented, with the corresponding sampling theorem and recovery algorithm. Section 3 presents results on synthetic pulse streams as well as on simulated US images. Concluding remarks are given in Section 4.

2. SIGNAL MODELS FOR PULSE STREAMS IN ULTRASOUND IMAGING

2.1. Ultrasound channel recovery from a pulse-stream model

From Equation (1), one may express the signal $m_p(t)$ as $m_p(t) = (s * h)(t)$, where $s(t) = \sum_{k=1}^{K} a_k \delta\left(t - t_p^k\right)$ and $h(t)$ is the pulse.

Let us consider that the signal $m_p(t)$ is sampled at a rate f_s, leading to N samples $m_p\left(t^i\right)$, with $t^i = t^0 + i/f_s$ for $i \in \{1, \ldots, N\}$.

The vector $\boldsymbol{m}_p = \left[m_p\left(t^1\right), \ldots, m_p\left(t^N\right)\right]^T \in \mathbb{R}^N$ belongs to the pulse-stream model $\mathcal{M}^{z}_{K,F}$ where F denotes the size of the support of $\boldsymbol{h} \in \mathbb{R}^N$, supposed to be small compared to N and K the number of point-scatterers.

Thus, one may be able to sample US signals at a rate dictated by Hedge and Baraniuk [7] while ensuring a perfect recovery. Moreover, since the pulse is supposed to be known, the following convex problem can be solved to retrieve $\boldsymbol{m}_p$ from noisy measurements $\boldsymbol{y} = \Phi \boldsymbol{m}_p + \boldsymbol{n}$, with $\Phi \in \mathbb{R}^{M \times N}$ a Gaussian *i.i.d.* matrix:

$$\min_{\bar{\boldsymbol{s}}} \|\bar{\boldsymbol{s}}\|_1 \text{ subject to } \|\boldsymbol{y} - \Phi \mathsf{H} \bar{\boldsymbol{s}}\|_2 \leq \epsilon, \tag{4}$$

where H is a circulant matrix which contains time-shifted replicas of the pulse, $\boldsymbol{m}_p = \mathsf{H}\boldsymbol{s}$, $\boldsymbol{s}$ is the K-sparse spike train and ϵ is a higher bound of the ℓ_2-norm of the noise.

2.2. Multi-channel ultrasound pulse-stream model

The model described in Section 2.1 is suited to single channel reconstructions. However, such a model does not account for inter-channel dependencies, which are self-evident in state-of-the-art US imaging configurations (see Figure 1). By taking into account such dependencies, one may be able to decrease the number of measurements required to reconstruct US signals. The following theorem precises the way the dependencies between two channels may be expressed.

Theorem 1 (Two-channel scenario)**.** *The support $\sigma(\boldsymbol{s}_i)$ of the spike train $\boldsymbol{s}_i$ corresponding to the sensor located at a distance Δ_{ij} from the sensor j, whose spike train is $\boldsymbol{s}_j$, has the following property:*

$$\sigma(\boldsymbol{s}_i) \subset S_{ij},$$

where $S_{ij} := \bigcup_{k=1}^{K} \Omega_k^{ij}$ is a union of $2D_{ij}$-dimensional subspaces Ω_k^{ij} defined by:

$$\Omega_k^{ij} := \{\{k - D_{ij}, \ldots, k + D_{ij}\},\ k \in \sigma(\boldsymbol{s}_j)\},$$

where $D_{ij} = \lceil f_s \Delta_{ij}/c \rceil$.

In the above theorem, $\lceil . \rceil$ designates the round value.

Proof. Let us suppose that $x_j(t) = \sum_{k=1}^{K} a_k \delta\left(t - t_j^k\right)$ and $x_i(t) = \sum_{k=1}^{K} a_k \delta\left(t - t_i^k\right)$. From Equation (2), one may deduce the following:

$$\begin{aligned} t_j^k &= t_{Tx}\left(\boldsymbol{r}^k\right) + t_{Rx}\left(\boldsymbol{r}^k, \boldsymbol{r}_{ts}^j\right) \\ &= t_{Tx}\left(\boldsymbol{r}^k\right) + \frac{\|\boldsymbol{r}^k - \boldsymbol{r}_{ts}^j\|_2}{c} \\ &\leq t_{Tx}\left(\boldsymbol{r}^k\right) + \frac{\|\boldsymbol{r}^k - \boldsymbol{r}_{ts}^i\|_2}{c} + \frac{\Delta_{ij}}{c} \\ &\leq t_i^k + \frac{\Delta_{ij}}{c}. \end{aligned}$$

Reversely, one can deduce that $t_j^k \geq t_i^k - \frac{\Delta_{ij}}{c}$, which leads to $t_i^k \in \left[t_j^k - \frac{\Delta_{ij}}{c}, t_j^k + \frac{\Delta_{ij}}{c}\right]$. Thus, by multiplying by f_s, one may deduce that:

$$\forall l \in \sigma(\boldsymbol{s}_i), \exists p \in \sigma(\boldsymbol{s}_j) \mid l \in \{p - D_{ij}, \ldots, p + D_{ij}\}, \tag{5}$$

where $D_{ij} = \lceil f_s \Delta_{ij}/c \rceil$. Generalizing Equation (5) to the support of $\sigma(\boldsymbol{s}_i)$, one may retrieve the result of Theorem 1. □

Theorem 1 states that the support of $\boldsymbol{s}_i$ is a union of K $2D_{ij}$-dimensional subspaces located around the support $\sigma(\boldsymbol{s}_j)$ of the signal received at sensor j. The dimension of each subspace depends on the distance between the sensors.

We can go further than the two-channel scenario by considering that we have prior knowledge on multiple channels. In this case, the following theorem holds.

Theorem 2 (Multi-channel scenario)**.** *The support $\sigma(\boldsymbol{s}_i)$ of the spike train $\boldsymbol{s}_i$ corresponding to the sensor located at distances $(\Delta_{ij})_{j=1}^{n}$ from a set of n sensors, whose spike trains are $(\boldsymbol{s}_j)_{j=1}^{n}$, has the following property:*

$$\sigma(\boldsymbol{s}_i) \subset S,$$

where $S := \bigcap_{j=1}^{n} S_{ij}$ is the intersection of the spaces S_{ij} defined in Theorem 1.

Proof. This is a simple generalization of Theorem 1. Let us denote as $(\boldsymbol{s}_j)_{j=1}^n$ the spike trains associated with the n considered sensors. Then, Theorem 1 states that:

$$\forall j \in \{1,\dots,n\},\ \sigma(\boldsymbol{s}_i) \in S_{ij} \Leftrightarrow \sigma(\boldsymbol{s}_i) \in \bigcap_{j=1}^{n} S_{ij}.$$

□

In this case, the support $\sigma(\boldsymbol{s}_i)$ is included into a smaller subspace, taking into account the dependencies between the considered sensor and the n other ones. We use the result of Theorem 2 to define the multi-channel US pulse-stream model as:

$$\mathcal{U}^z_{K,F} := \left\{ \boldsymbol{z} \in \mathbb{R}^N : \boldsymbol{z} = \boldsymbol{s} * \boldsymbol{h} \mid \boldsymbol{s} \in \mathcal{M}_K,\ \sigma(\boldsymbol{s}) \subset S \right\}, \quad (6)$$

where $\boldsymbol{h}$ is supposed to be known.

2.3. Sampling theorem of multi-channel ultrasound pulse-stream

The multi-channel US pulse-stream model has an additional structure compared to the general pulse-stream model which can be exploited in order to reduce the sampling rate requirements for signals belonging to $\mathcal{U}^z_{K,F}$. The theorem hereafter makes this precise and sets the sampling requirements for multi-channel US pulse-stream signals.

Theorem 3. *Suppose that $\mathcal{U}^z_{K,F}$ is the multi-channel ultrasound pulse-stream model defined in Equation (6). Let $t > 0$ and $\delta > 0$. Choose a $M \times N$ i.i.d Gaussian matrix Φ with*

$$M \geq \mathcal{O}\left((K+F)\ln\left(\frac{1}{\delta}\right) + K\left(1+\log\left(\frac{|S|}{K}\right)\right) + t \right).$$

Then Φ satisfies the following property with probability $1-e^{-t}$: $\forall \boldsymbol{z}_1, \boldsymbol{z}_2 \in \mathcal{U}^z_{K,F}$,

$$(1-\delta)\|\boldsymbol{z}_1 - \boldsymbol{z}_2\|^2 \leq \|\Phi\boldsymbol{z}_1 - \Phi\boldsymbol{z}_2\|^2 \leq (1+\delta)\|\boldsymbol{z}_1 - \boldsymbol{z}_2\|^2.$$

In the theorem above $|S|$ denotes the cardinality of the set S.

Proof. The proof is based on Theorem 1 of [7]. Suppose that $\boldsymbol{z} \in \mathcal{U}^z_{K,F}$, then, $\boldsymbol{z} \in \mathcal{M}^z_{K,F}$. From [7], one may set the bound M as:

$$M \geq \mathcal{O}\left((K+F)\ln\left(\frac{1}{\delta}\right) + \log(L_K L_F) + t \right) \quad (7)$$

where $t > 0$. When $\boldsymbol{h}$ is known, $L_F = 1$. Moreover, if we consider that $\sigma(\boldsymbol{s}) \subset S$, then the following inequality holds:

$$L_K \leq \binom{|S|}{K} \approx \left(\frac{e|S|}{K}\right)^K$$
$$\Leftrightarrow \log(L_K) \leq K\left(1+\log\left(\frac{|S|}{K}\right)\right).$$

Introducing the above results in Equation (7) leads to the results of Theorem 3. □

The main benefit of Theorem 3 is that, as described by Hedge and Baraniuk [7], the number of samples only depends on the size of the support rather than the size of the signal. The number of measurements also scales with $K+F$, which is consistent with the pulse-stream model.

2.4. Recovery of multi-channel ultrasound pulse-stream

The signal $\boldsymbol{m} = \boldsymbol{s} * \boldsymbol{h}$, $\boldsymbol{m} \in \mathcal{U}^z_{K,F}$, can be recovered by solving the following problem:

$$\min_{\bar{\boldsymbol{s}}_{|S}} \|\bar{\boldsymbol{s}}_{|S}\|_1 \text{ subject to } \|\boldsymbol{y} - \Phi\mathsf{H}\mathsf{W}_S\bar{\boldsymbol{s}}_{|S}\|_2 \leq \epsilon, \quad (8)$$

where $\bar{\boldsymbol{s}}_{|S}$ represents the entries of $\boldsymbol{s}$ corresponding to the set of indices S and $\mathsf{W}_S \in \mathbb{R}^{N\times|S|}$ is a selection matrix. Problem (8) is solved using state-of-the-art convex optimization algorithms.

3. EXPERIMENTS

We now present the results of experiments that validate the proposed approach and show its benefits. In all the experiments, Problem (8) is solved using the alternating direction methods of multipliers (ADMM) [12].

3.1. Synthetic $1D$-pulse streams

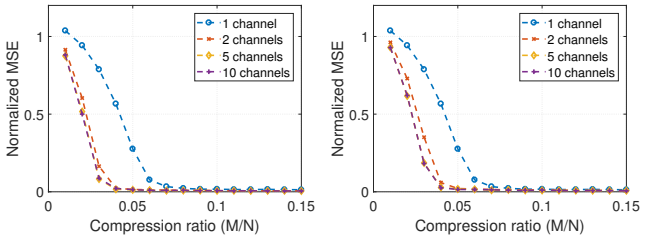

(a) (b)

Fig. 2: Normalized MSE for (a) $\Delta = 0.31$ mm (phased-array) and (b) $\Delta = 0.62$ mm (linear-array) vs. the compression ratio (M/N) for the proposed method for 1-, 2-, 5- and 10-channel scenarios. Signals parameters: $N = 2000$, $F = 31$, $K = 20$.

First, $K = 20$ point-scatterers with random amplitudes and positions $\boldsymbol{r}^k = \left[x^k, z^k\right]^T$ for k between 1 and K are generated. 10 sensors are considered, with an inter-sensor spacing of Δ. Spike trains of length $N = 2000$ are deduced from $\boldsymbol{r}^k$ and Δ using Equation (2), where $t_{Tx}\left(\boldsymbol{r}^k\right) = z^k/c$. The synthetic $1D$-pulse streams are generated by convolving the 10 spike trains with a pulse $h(t)$ where the excitation signal is set to $e(t) = \sin(2\pi f_0 t)$, with $t \leq 1/f_0$, and $h_{ae}(t) = h_{ea}(t) = w(t)\sin(2\pi f_0 t)$, where $w(t)$ is a Hanning window and $t \leq 2/f_0$. The central frequency f_0 is chosen to be 5 MHz and the sampling frequency f_s is set to 30 MHz, leading to $F = 31$.

Figure 2 displays the averaged results of a Monte-Carlo simulation over 1000 trials of the ADMM algorithm. Each trial was conducted by randomly generating the amplitudes and positions of the K point-scatterers, the Gaussian *i.i.d* matrix $\Phi \in \mathbb{R}^{M\times N}$ and by reconstructing the raw data $\boldsymbol{m}$ of one sensor from different values of M/N. 1-channel as well as multi-channel scenarios are considered. For the multi-channel scenarios, prior knowledge on the support of the spike trains of $1, 4$ and 9 neighbouring sensors of the sensor of interest are considered. Figure 2a and 2b show the normalized mean squared error (NMSE), calculated as $\|\boldsymbol{m} - \boldsymbol{m}^\star\|_2/\|\boldsymbol{m}\|_2$, where $\boldsymbol{m}$ is the reference and $\boldsymbol{m}^\star$ the estimate, for two different inter-sensor spacings, namely 0.31 mm (one wavelength) and 0.62 mm (two wavelengths). Concerning the optimization algorithm, the maximum number of iterations is set to 1000 and $\epsilon = 0$.

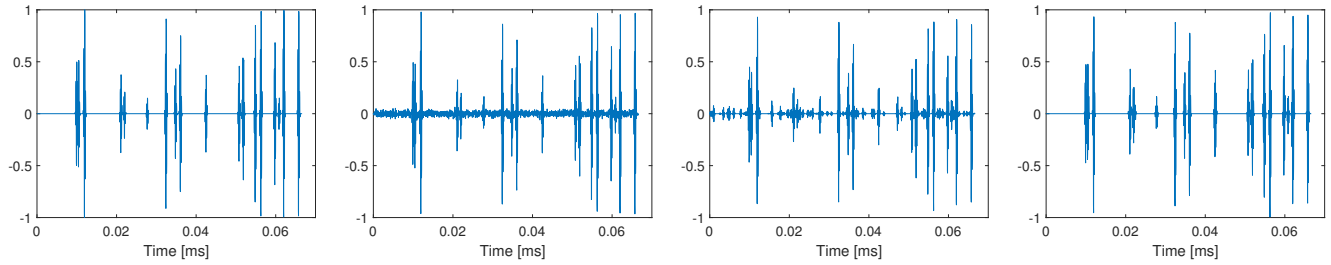

(a) (b) (c) (d)

Fig. 3: (a) Original signal (b) Noisy signal (SNR =40 dB) (c) Recovered estimate from $M = 160$ measurements in a 1-channel scenario (d) Recovered estimate from $M = 160$ measurements in a 5-channel scenario.

From Figure 2, it is clear that the multi-channel configurations outperform the 1-channel configuration. Regarding Figures 2a and 2b, it can be noticed that, for a higher inter-sensor spacing, the 5-channel and 10-channel scenarios outperform the 2-channel scenario. Indeed, when the spacing is higher, the dimension of the subspaces S_i is increased and the dimensionality reduction induced by Theorem 2 has a higher impact.

Figure 3 demonstrates that the proposed algorithm is robust to small amount of noise (SNR = 40 dB). For this experiment, the settings are the same as the ones used for the noiseless experiment. A small amount of Gaussian noise is added to the element raw-data of each sensor, leading to the signal displayed on Figure 3b. Figures 3c and 3d show the recovered signals for the 1-channel and 5-channels scenarios, respectively, for a number of measurements $M = 160$. It can be seen that the signal recovered from the 5-channel scenario is closer to the original signal than the one recovered from the 1-channel scenario.

3.2. *In vivo* ultrasound images

Element raw-data of an *in vivo* carotid, for 1 PW insonification with normal incidence, have been acquired with an Ultrasonix scanner (Ultrasonix Analogic Ultrasound, Richmond, BC, Canada), equipped with a linear probe composed of 128 transducer-elements, working at 5 MHz with 100 % bandwidth, with an inter-sensor spacing of 0.46 mm. The sampling frequency has been set to 40 MHz.

After acquisition, the element raw-data are imported on MATLAB (The Mathworks, Natic, MA) and compressed using a Gaussian *i.i.d* matrix $\mathbf{\Phi} \in \mathbb{R}^{M \times N}$, with a compression ratio $M/N = 0.06$, with $N = 1519$. The pulse is supposed to be known and equal to the one described in Section 3.1. In the multi-channel scenario, a sequential reconstruction is achieved where each channel is recovered with prior knowledge on the support of the spike train corresponding to the neighbouring channel (obtained from the previous reconstruction). Concerning the optimization algorithm, the maximum number of iterations is set to 2000 and $\epsilon = 0.3\|\boldsymbol{y}\|_2$.

Once the raw data are reconstructed from compressed measurements, standard US beamforming is applied to generate the radio-frequency (RF) image. The envelope is extracted through Hilbert transform, normalized and log-compressed (dynamic range of 40 dB) to obtain the B-mode image.

Figure 4, which displays the recovered B-mode images, shows an increase of the image quality in the multi-channel scenario. This increase is quantified by a difference of 1 dB in the peak-signal-to-noise ratio (PSNR) between the 1- and the multi-channel reconstructions.

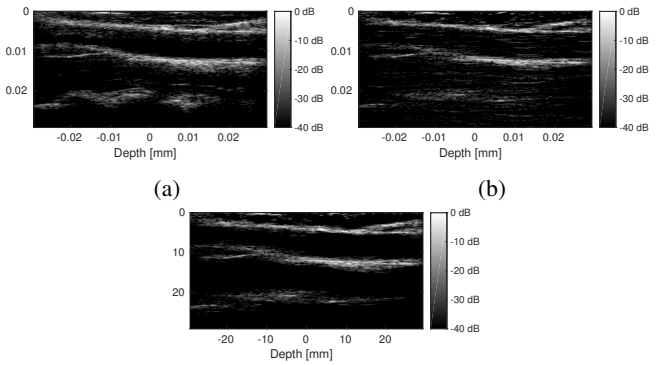

(a) (b)

(c)

Fig. 4: (a) Original B-mode image of the carotid; Recovered B-mode image from $M = 91$ measurements (b) in a 1-channel scenario (PSNR = 28.4 dB); (c) in a 2-channels scenario (PSNR = 29.4 dB).

4. CONCLUSION

In this paper, we have presented an extension of the pulse-stream model to ultrasound imaging. The proposed model, coined as *multi-channel US pulse-stream model*, accounts for the inter-sensor dependencies as an additional structure to the general pulse-stream model. This structure enables us to quantitatively estimate the number of random projections necessary to sample such signals. We also suggest a reconstruction method based on ℓ_1-minimization on the reduced signal support. We have illustrated its benefits on synthetic $1D$-pulses as well as on *in vivo* ultrasound images.

5. REFERENCES

[1] Mickael Tanter and Mathias Fink, "Ultrafast imaging in biomedical ultrasound," *IEEE Trans. Ultrason. Ferroelectr. Freq. Control*, vol. 61, no. 1, pp. 102–119, jan 2014.

[2] Tanya Chernyakova and Yonina C. Eldar, "Fourier-domain beamforming: the path to compressed ultrasound imaging," *IEEE Trans. Ultrason. Ferroelectr. Freq. Control*, vol. 61, no. 8, pp. 1252–1267, aug 2014.

[3] Ronen Tur, Yonina C. Eldar, and Zvi Friedman, "Innovation rate sampling of pulse streams with application to ultrasound imaging," *IEEE Trans. Signal Process.*, vol. 59, no. 4, pp. 1827–1842, apr 2011.

[4] J.A. Jensen and N.B. Svendsen, "Calculation of pressure fields from arbitrarily shaped, apodized, and excited ultrasound transducers," *IEEE Trans. Ultrason. Ferroelectr. Freq. Control*, vol. 39, no. 2, pp. 262–267, mar 1992.

[5] Gabriel Montaldo, Mickaël Tanter, Jérémy Bercoff, Nicolas Benech, and Mathias Fink, "Coherent plane-wave compounding for very high frame rate ultrasonography and transient elastography," *IEEE Trans. Ultrason. Ferroelectr. Freq. Control*, vol. 56, no. 3, pp. 489–506, mar 2009.

[6] Clement Papadacci, Mathieu Pernot, Mathieu Couade, Mathias Fink, and Mickael Tanter, "High-contrast ultrafast imaging of the heart," *IEEE Trans. Ultrason. Ferroelectr. Freq. Control*, vol. 61, no. 2, pp. 288–301, feb 2014.

[7] Chinmay Hegde and Richard G. Baraniuk, "Sampling and recovery of pulse streams," *IEEE Trans. Signal Process.*, vol. 59, no. 4, pp. 1505–1517, apr 2011.

[8] M. Vetterli, P. Marziliano, and T. Blu, "Sampling signals with finite rate of innovation," *IEEE Trans. Signal Process.*, vol. 50, no. 6, pp. 1417–1428, jun 2002.

[9] Emmanuel J. Candès and M.B. Wakin, "An introduction to compressive sampling," *IEEE Signal Process. Mag.*, vol. 25, no. 2, pp. 21–30, mar 2008.

[10] Farid M Naini, Rémi Gribonval, Laurent Jacques, and Pierre Vandergheynst, "Compressive sampling of pulse trains: Spread the spectrum!," in *IEEE Int. Conf. Acoust. Speech Signal Process.*, apr 2009, pp. 2877–2880.

[11] Grigorios Tsagkatakis, Panagiotis Tsakalides, Arnaud Woiselle, Marc Bousquet, George Tzagkarakis, and Jean-Luc Starck, "Compressed sensing reconstruction of convolved sparse signals," in *IEEE Int. Conf. Acoust. Speech Signal Process.*, may 2014, pp. 3340–3344.

[12] Stephen Boyd, "Distributed optimization and statistical learning via the alternating direction method of multipliers," *Found. Trends Mach. Learn.*, vol. 3, no. 1, pp. 1–122, jan 2011.